

Vortex Instability, Generation of New Vortices, and Onset of Turbulence in Superfluid $^3\text{He-B}$

V.B. Eltsov,^{1,2} A.P. Finne,¹ R. de Graaf,¹ R. Hänninen,¹ J. Kopu,¹ M. Krusius,¹ and R.E. Solntsev¹

¹*Low Temperature Laboratory, Helsinki University of Technology, P.O.Box 2200, 02015 HUT, Finland*

²*Kapitza Institute for Physical Problems, Kosyginia 2, 119334 Moscow, Russia*

(Dated: February 8, 2020)

Vortex dynamics in superfluid $^3\text{He-B}$ is distinguished by an abrupt transition to turbulence which is caused by a strongly temperature dependent mutual friction dissipation $\alpha(T)$. Above $0.6 T_c$ dynamic processes are vortex number conserving. At lower temperatures a vortex moving in applied flow with respect to the container walls may become unstable, create new vortices, and start thereby turbulence. This single-vortex instability can be monitored in a rotating long cylinder in the temperature regime where turbulence starts. By comparing NMR measurements to numerical calculations, we study the expansion of newly created vortices to rectilinear lines, while the instability generates new vortices at a low rate ~ 1 vortex/s, before turbulence sets in.

PACS numbers: 67.57.Fg, 47.32.-y, 67.40.Vs

Vortices in superfluids are topologically stable structures of a coherent order parameter field with a fixed quantized circulation of superflow (κ). How are new vortices generated from existing ones under the influence of externally applied superfluid counterflow (cf)? The common view holds that this happens via loop formation and reconnections in bulk superfluid, as seen in well-developed thermal cf turbulence of superfluid $^4\text{He-II}$ [1]. However, as explained by Schwarz [2], to start or sustain turbulence this is not sufficient if you consider flow applied along a circular tube, for instance. He suggested for this vortices pinned in “vortex-mill” configurations which continuously inject new vortex loops downstream in the applied flow. It is now known from rotating measurements on $^3\text{He-B}$ in smooth-walled cylinders, where no permanently pinned vortices exist [3], that turbulence can suddenly start from one single seed vortex ring which is externally introduced in the rotating vortex-free cf [4]. Standard numerical vortex-dynamics calculations do not confirm that a single vortex ring would become unstable in applied bulk flow at finite vortex damping $\alpha(T)$, except if the flow is spatially strongly inhomogeneous [5].

A more recent explanation [6] asserts that a vortex ring may become unstable while colliding with the container wall and reconnecting there. A suitably oriented reconnection kink excites an expanding Kelvin wave loop which in turn reconnects at the wall and thereby forms a new independent vortex. In this way a topologically stable line vortex can generate new vortices and build up a density where inter-vortex interactions become possible and start bulk turbulence. The instability sets in when the damping $\alpha(T)$ drops below $\alpha(T) \lesssim 1$ at low temperatures [7]. In practice the instability is noticed as a sudden transition to turbulence, with a sharp onset temperature T_{on} [8].

The transition to turbulence T_{on} depends primarily on $\alpha(T)$, but also weakly on other factors which influence the likelihood of achieving locally the vortex density re-

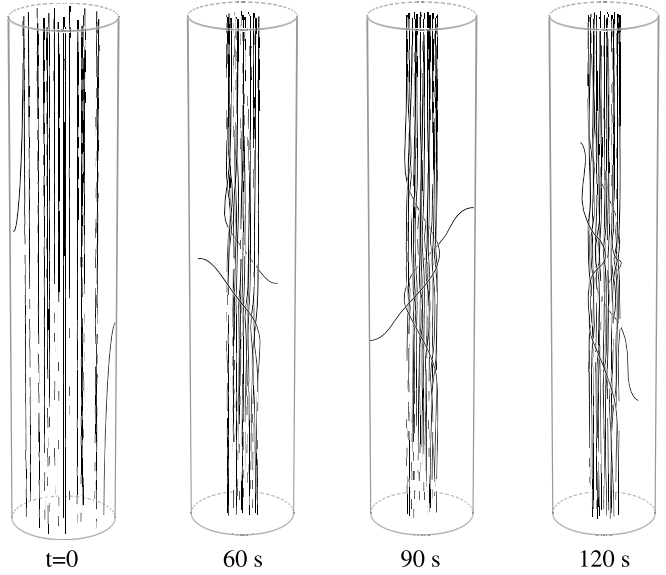


FIG. 1: Numerical calculation of vortex evolution in a rotating cylinder of $^3\text{He-B}$: Rotation is suddenly increased at $t = 0$ from $\Omega_i \approx 0.03 \text{ rad/s}$ to $\Omega_f = 0.2 \text{ rad/s}$, with 22 vortices in the sample (of which two in the outermost ring of vortices have been bent to the cylindrical wall to mimic an inclined cylinder). In the later snapshots at Ω_f , the two short vortices expand towards the top and bottom end plates of the cylinder. Parameters: $R = 3 \text{ mm}$, $L = 30 \text{ mm}$, $P = 29.0 \text{ bar}$, and $T = 0.4 T_c$ (which corresponds to $\alpha = 0.18$ and $\alpha' = 0.16$ [10]).

quired for turbulence to start. Most important is (i) the applied cf velocity $\mathbf{v} = \mathbf{v}_n - \mathbf{v}_s$, the difference between the velocities of the normal and superfluid fractions in the two-fluid model, (ii) the number and configuration of the injected seed vortices, and (iii) the sample geometry. Here we examine the evolution and motions of vortices in a rotating cylinder, while the seed vortices become unstable and generate more vortices via the *single-vortex instability* in the onset temperature regime $T \sim T_{\text{on}}$.

Numerical illustration: To visualize the motion of

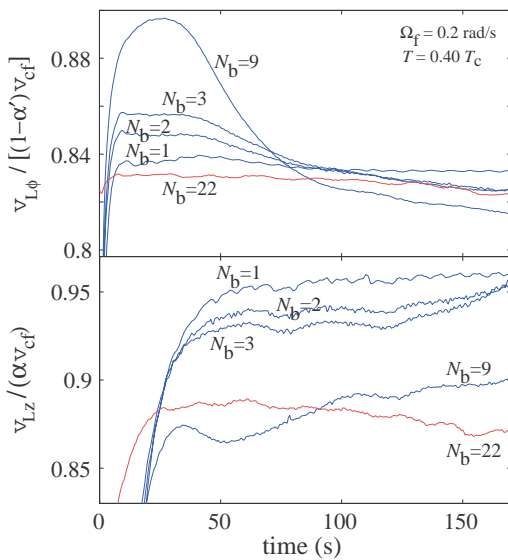


FIG. 2: Comparison of longitudinal v_{Lz} (bottom) and azimuthal $v_{L\phi}$ (top) velocities with different numbers of vortices N_b expanding as one bundle in the setup of Fig. 1. With 22 vortices in total, 1, 2, 3, or 9 vortices of equal initial length $0.4 L$ have been bent both on the top and bottom to the cylindrical wall, to mimic a tilted cylinder, as in Fig. 1. The spiraling motion both upwards and downwards along the rotating column is then calculated as function of time. The average velocity of the vortex ends on the cylindrical wall in the upward and downward moving bundles is plotted during the time needed to reach the respective end plate. The actual velocity is the number on the vertical scale times $\alpha v(\Omega_f, R, N)$ or $(1 - \alpha')v(\Omega_f, R, N)$, where $N = 22 - N_b$. $N_b = 22$ is the case where all 22 vortices are bent at one end only to the wall and a vortex front expands towards the other end in vortex-free cf with $v = \Omega R$.

seed vortices in rotating flow, a calculation is shown in Fig. 1 of two curved vortices which connect to the cylindrical wall. The calculations are performed using the numerical techniques described in Ref. 9. For simplicity, rotation Ω is increased in step-like manner at $t = 0$ from the equilibrium vortex state at $\Omega_i \neq 0$ to a final stable value Ω_f . The $N = 20$ rectilinear vortices are thereby compressed to a central cluster with areal density $n_v = 2\Omega_f/\kappa$ by the surrounding cf, which outside the cluster has the velocity $v(\Omega_f, r, N) = \Omega_f r - \kappa N/(2\pi r)$. The two short vortices expand in the cf in spiral motion towards the top and bottom end plates, respectively. The velocity \mathbf{v}_L of a vortex line element with tangent $\hat{\mathbf{s}}$ is given by

$$\mathbf{v}_L = \mathbf{v}_s + \alpha \hat{\mathbf{s}} \times (\mathbf{v}_n - \mathbf{v}_s) - \alpha' \hat{\mathbf{s}} \times [\hat{\mathbf{s}} \times (\mathbf{v}_n - \mathbf{v}_s)], \quad (1)$$

where α is the dissipative and α' the reactive mutual friction coefficient. A simple model of the motion of the two short vortices is obtained by examining the velocities of their end points on the cylindrical wall. Since the vortex end is perpendicular to the cylindrical wall, it has a longitudinal velocity $v_{Lz} = \alpha v(\Omega_f, R, N)$ and an azimuthal

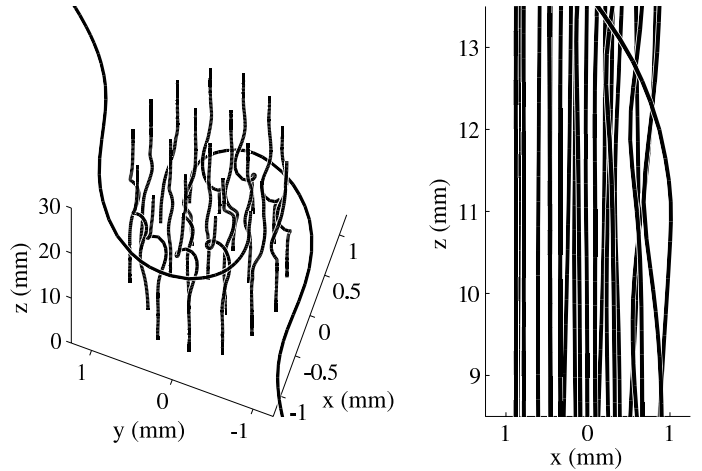


FIG. 3: (Left) Rotating cylinder of Fig. 1 at $t = 60$ s, viewed at an angle deviating by 3° from vertical. Helical Kelvin waves are induced on the vortex lines in the cluster by the two vortices spiraling outside the cluster. In the early stage of the expansion ($t = 60$ s), the waves start at half-height of the sample where the two short vortices merge with the cluster (see Fig. 1). (Note that only the central part of the sample is shown in this figure in the x and y directions.) (Right) Side view through the vortex cluster. A vortex spiraling around the cluster induces radial displacements on the outermost vortices within the cluster. The displacements start longitudinally propagating Kelvin waves on these vortices.

component $v_{L\phi} = (1 - \alpha')v(\Omega_f, R, N)$. These are here expressed in the rotating coordinate system so that $v_{L\phi}$ points in the opposite direction from the rotation of the container.

Evidently other parts of the vortex also contribute to its motion, in particular its curvature where it connects to the cylindrical wall. However, it turns out that the end point velocity is an approximate guide for the expansion of a single vortex in vortex-free rotation. For comparison, the calculated velocities of the two vortex ends in Fig. 1 are $v_{Lz} \approx 0.84 \alpha \Omega R \approx 0.96 \alpha v$ and $v_{L\phi} \approx 0.73(1 - \alpha')\Omega R \approx 0.83(1 - \alpha')v$. The wave length of the trajectory is $\lambda = 2\pi R v_{Lz}/v_{L\phi} \approx 5$ mm and the period $p = 2\pi R/v_{L\phi} \approx 50$ s. In Fig. 2 the velocities v_{Lz} and $v_{L\phi}$ have been plotted for different number of vortices in spiral expansion. The initial starting state of these calculations is one where the specified number (N_b) of nearest-neighbor vortices is bent to the cylindrical wall to the same height. This is done as shown in Fig. 1 on the left (at $t = 0$), with one set of vortices having their second end on the top plate and another set with the second end on the bottom plate. When rotation is increased to Ω_f , the curved vortices start their spiral propagation along the cylinder towards their respective end plates.

Interestingly, the vortices expanding upwards, for instance, which initially start off in close proximity of each other, remain a close bundle during their spiral motion. The calculations display relatively small spread in velocities both as a function of time and also among the

different vortices within the bundle, when N_b is small (see curves with $N_b \lesssim 3$ in Fig. 2). This is the case especially during the late part of the expansion, when the spiralling vortices have reached a state of steady propagation along the cylinder. For better comparison with our measurements the number of vortices should be increased in the central cluster from that in Figs. 1 and 2. This calls for time-consuming calculations which are partly in progress. Preliminary tests suggest that the result for the azimuthal velocity $v_{L\phi}/[(1 - \alpha')v]$ drops to lower values than in Fig. 2. The limiting case is the expansion of approximately the equilibrium number of vortices N_{eq} into a vortex-free section of the rotating cylinder (where no vortex cluster yet exists). At present temperatures $0.40 - 0.45 T_c$, these expanding $\lesssim N_{eq}$ vortices form a sharp front which maintains its constant narrow width during the spiraling propagation along the cylinder [11]. According to numerical calculations [8], the azimuthal velocity of the front is $v_\phi \approx \frac{1}{2}(1 - \alpha')\Omega R$, when the number of vortices in the front is large ($\gtrsim 200$). The second note about Fig. 2 is that both v_{Lz} and $v_{L\phi}$ are rather insensitive to the number of vortices N_b in the bundle when N_b is small, as seen in Fig. 2. This is also the case in our measurements.

While spiraling around the cluster of rectilinear lines, the two curved vortices in Fig. 1 may reconnect with each other or with the outermost lines in the cluster. These reconnections do not increase the vortex number. As seen in Figs. 1 and 3, a spiraling vortex distorts the cluster by inducing propagating helical Kelvin waves on the vortex lines, which results in oscillations of the cluster around its equilibrium position [12]. From the above simulation calculation we find that the amplitude of the vortex waves is comparable to the inter-vortex distance in the cluster, $\sim 1/\sqrt{n_v}$, and that initially the wavelength and period of the Kelvin waves have similar values as calculated above for the precessing vortex motion. In this calculation it appears that the spiral vortex motion and the Kelvin waves, which it induces, initially combine to produce the precession of the “flare-out order parameter texture” [8, 14] around its equilibrium location. This is the signal which we interpret to correspond to the oscillating component in the measured NMR response below.

Finally we note that the vortices in our numerical calculations are less likely to become unstable and generate new vortices than what is observed in our measurements. Thus Figs. 1 and 2 illustrate the experimental situation above T_{on} where no increase in vortex number occurs, although the measured T_{on} is higher than $0.40 T_c$, the temperature of the present calculations. The most likely section of a vortex to become unstable during the expanding motion is the curved piece ending on the cylindrical wall since it resides in the maximum flow $|\mathbf{v}(R)|$. In contrast, rectilinear lines we find to remain stable in our measurements even in accelerating rotation above temperatures

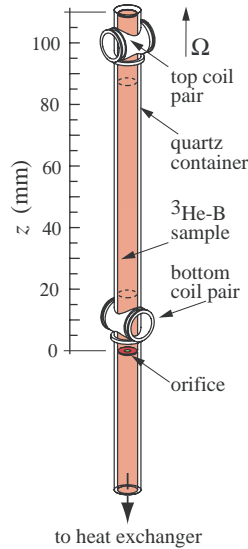


FIG. 4: Sample cylinder with detector coils.

$\gtrsim 0.30 T_c$.

Experiment: We record non-invasively the NMR line shape with detector coils at both ends of a cylinder with radius $R = 3$ mm and length $L = 110$ mm (Fig. 4). Both detectors consist of a pair of coils, 9 mm in diameter with their axes aligned transverse to the cylinder [13]. Flow is applied by rotating the cylinder with angular velocity Ω with the sample at a pressure of 29.0 bar. The NMR line shape is dominated by a large cf peak which is shifted from the Larmor frequency [14]. Its height decreases with the number of vortices N in the central cluster. The conversion from peak height to corresponding N can be obtained from calculations of the order parameter texture or from measurements. The present measurements are started from a state with large N at $\Omega \gtrsim 1$ rad/s which is decelerated at a rate 0.01 rad/s² to zero. Zero rotation is then maintained for a period Δt , to allow vortices to annihilate, with the exception of a few remaining dynamic remnants [3]. The final step is to increase Ω at some fixed rate to Ω_f , where it is kept constant while the buildup in the number of vortex lines $N(t)$ in the central cluster is recorded as a function of time.

Single vortex instability: Well above the onset temperature $T > T_{on}$, the cf peak height settles to a stable value and remains then constant at Ω_f . Well below onset $T < T_{on}$, the cf peak collapses to zero as the equilibrium vortex state is formed. In the onset regime $T \sim T_{on}$, both types of behavior occur randomly [3], but if the equilibrium vortex state is the final state, then the collapse of the cf peak is preceded by an initial slow decrease in peak height. This almost linear reduction in height we associate with the single-vortex instability. It can only be distinguished in the onset regime since at lower temperatures turbulence follows too rapidly. These features have been examined in Ref. [6]. Here we focus on a rare

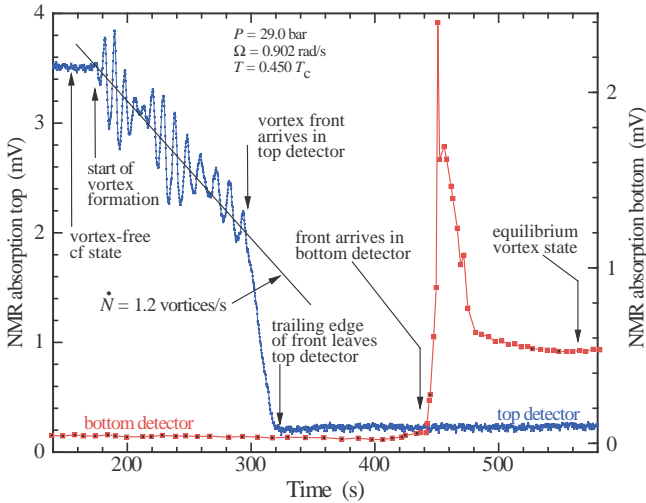


FIG. 5: Precursory vortex formation which terminates in a sudden turbulent burst. The oscillating cf peak height is recorded with the top detector while the bottom coils monitor the NMR absorption peak close to the Larmor edge. Both signals are shown versus time, with $t = 0$ marking the moment when $\Omega_f = 0.90$ rad/s is reached. The time interval between the collapse in the top and the sudden rise in the bottom responses measures the longitudinal motion while the oscillation frequency gives the azimuthal precession. The former is controlled by $\alpha = 0.33$ and the latter by $1 - \alpha' = 0.76$ (at $T = 0.45 T_c$, from Ref. [10]).

type of oscillating response in the cf peak height decay. It illuminates the spiral motion of the expanding vortices which are generated by the single-vortex instability.

Oscillatory peak height response : The oscillating cf peak height in Fig. 5 is recorded with the top detector as a function of time at constant T and Ω . Initially, after a waiting period $\Delta t = 21.5$ min at zero rotation we increased Ω at a low rate $4 \cdot 10^{-3}$ rad/s 2 to $\Omega_f = 0.90$ rad/s. This is the starting situation in Fig. 5. Three minutes later after reaching Ω_f , the cf peak height starts oscillating and simultaneously decreases in amplitude. The average slope of the decreasing peak height corresponds to a vortex formation rate $\dot{N} \approx 1.2$ vortices/s, according to the measured calibration. In this example the source of vortex formation is not in control. Evidently vortex formation should have started from a single remanent vortex which did not annihilate at zero rotation. However, it remains unexplained how the long 3 min delay comes about, before the slow reduction in the cf peak height starts.

After about 120 s the oscillating cf peak collapses: the turbulent burst has occurred close to the top coil. The central cluster within the top coil contains now some 140 vortices and in addition many vortices are in different stages of spiral expansion. The turbulent burst increases the vortex number locally to the equilibrium value of $N_{eq} \approx 840$. These additional vortices then form a propagating vortex front, which travels along the cylinder and

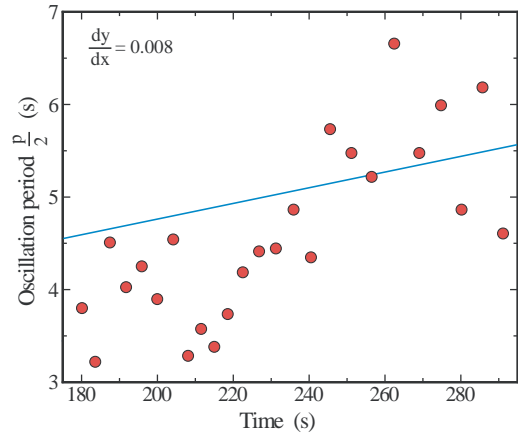


FIG. 6: Time difference between the maxima and minima in the oscillating cf peak height in Fig. 5. The line is obtained from that in Fig. 5 using Eq. (2).

removes the macroscopic cf generated by the rotation. Behind the front the expanding vortices are wound in a helically twisted configuration which relaxes only slowly [11].

The second trace in Fig. 5 is the response from the bottom coil pair. This signal is recorded at a different location of the absorption line shape, by scanning the absorption maximum close to the Larmor edge [14]. Initially with cf corresponding to $\Omega \sim 0.9$ rad/s this signal is not sensitive to the buildup of the central vortex cluster, as shown by the almost constant absorption level at $t < 400$ s. However, a sharp absorption increase signals the arrival of the vortex front as it passes through the top edge of the bottom coils. This defines the propagation time $\tau_F \approx 145$ s for the vortex front to cover the distance $d \approx 80$ mm between the detectors. The longitudinal propagation velocity of the front has been found to approximate the single-vortex velocity $v_{Lz} \approx \alpha v(\Omega_f, R, N)$ at this temperature [15]. Estimating from here, we find $N \sim 230$ vortices to populate on average the central cluster at the time when the front travels along the column from the top to the bottom detectors. The absorption increase monitored by the bottom coils consists of a transient peak, which arises when the vortex front with the trailing twisted vortices passes through the coil pair, and of the stable final absorption level from the equilibrium vortex state, after the twist has relaxed [11].

Spiral vortex motion: The source for the oscillations in the cf peak height in Fig. 5 we attribute to the spiral vortex motion. The oscillating signal arises when the “flare-out” order parameter texture [8] precesses within the cylinder around its axially symmetric equilibrium position. The precession is driven by the spiral vortex motion. This is expected to have the frequency

$$f_\phi = \varepsilon (1 - \alpha') v(\Omega_f, R, N) / (2\pi R), \quad (2)$$

where $\frac{1}{2} \lesssim \varepsilon < 1$, depending on the number of vortices

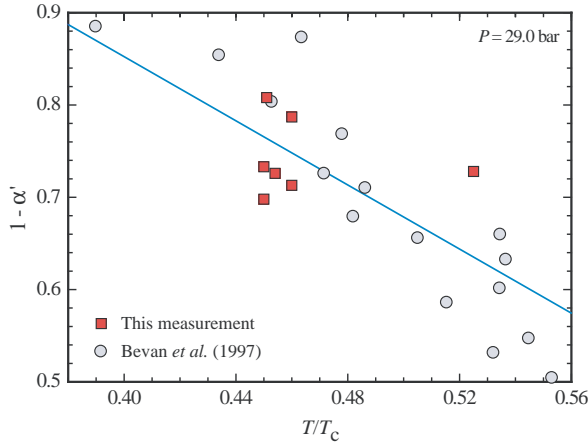


FIG. 7: Reactive mutual friction coefficient $1 - \alpha'$ versus temperature.

spiraling coherently in one bundle, as discussed above. If we assume $\varepsilon = \frac{1}{2}$, then we expect $f_\phi \approx 0.055$ Hz in the early stages when N is small. The sensitivity of the detector coil pair is not constant across the cross section of the sample, but increases towards the windings. This doubles the measured frequency from that of the azimuthally precessing asymmetry in the order parameter texture and thus $f_{\text{exp}} \approx 0.11$ Hz. In Fig. 6 it is seen that the measured oscillation period p is consistent with this estimate and that it continuously increases as the number of vortices N in the central cluster increases and the cf velocity $v(\Omega_f, R, N)$ decreases.

By comparing the measured f_{exp} and expected f_ϕ , we have extracted α' from seven cf peak decays which display a prolonged oscillatory response. In these cases the single-vortex instability proceeds typically at a rate $\dot{N} \sim 0.4 - 2$ vortices/s, while Ω_f is in the range $0.8 - 1.2$ rad/s. As seen in Fig. 7, the results agree with the measurements on $\alpha'(T)$ in Ref. 10. Here we have consistently assumed that $\varepsilon = \frac{1}{2}$. Because of the uncertainty about the value of ε , Fig. 7 is not presented as a measurement of $\alpha'(T)$. Rather it is a consistency test on our explanation of the unusual oscillatory NMR response, which is driven by spiral vortex motion and kept going by the single-vortex instability.

Discussion: The prolonged oscillatory response in the cf peak height in Fig. 5 is a rare event. To obtain this response, three preconditions have to be fulfilled: (1) New vortices have to be created at a slow rate. For this the temperature has to be in the vicinity of T_{on} where the single-vortex instability continues for longer periods, before the turbulent burst sets in and the vortex front is formed. (2) The wavelength of the spiral motion has to match the diameter of the detector coil. In Fig. 5 the longitudinal travel time of a vortex end through the detector is ~ 10 s which equals one full cycle of the azimuthal motion. The periodic oscillation cannot be resolved if the

detector is much larger than this in diameter. (3) The spiral motion of many vortices has to be coherent: the 13 beautiful oscillations in Fig. 5 cannot be attributed to a single vortex since the transit time for a vortex end to pass through the detector corresponds to one period only. Three features may help to create and preserve the coherent motion: (i) When a vortex end on the cylindrical wall creates a new loop, one end of the new loop starts spiraling close to the original end. (ii) The detector is close to one end of the cylinder and, assuming that the instability occurs randomly, almost all vortices approach the detector from the direction of the far end of the cylinder. (iii) In numerical calculations the evolving vortices, which start to spiral as a close bundle, tend to remain in a bunch while propagating along the cylinder.

Conclusion: Oscillating responses from precessing vortex motion have been reported before in He superfluids. A remarkable example is the unwinding of trapped circulation on a thin wire suspended along the axis of a cylindrical sample, known as the Vinen vibrating wire experiment [16]. In this report we have studied the precession of a vortex around a central cluster of vortex lines. Many details in our explanation of this unusual oscillatory response (Fig. 5) remain obscure, but the sudden appearance of this phenomenon at intermediate temperatures $\sim 0.45 T_c$ is a manifestation of the dynamics of quantized vortex lines as a function of mutual friction dissipation and of the single-vortex instability, in particular.

In He superfluids the single-vortex instability is the generic mechanism for generating new vortices, when (i) flow is applied in the presence of bounding walls, (ii) mutual friction dissipation $\alpha \lesssim 1$, and (iii) the density of active vortices is low. In $^4\text{He-II}$ the instability exists at almost all temperatures while in $^3\text{He-B}$ it is present only below $0.6 T_c$. In $^3\text{He-B}$ the instability can be identified experimentally around T_{on} , where it proceeds more slowly in time. In numerical calculations the events leading to the instability can be reconstructed when a vortex drifts in applied flow along an ideal wall and reconnects there [6].

Acknowledgements: This work was supported by the Academy of Finland, by ULTI research visits in the EU Transnational Access Programme FP6 (Contract RITA-CT-2003-505313), and the ESF research program COSLAB. We thank N.B. Kopnin, V.V. Lebedev, E.V. Thuneberg, and G.E. Volovik for valuable discussions. RH thanks the Foundation for the Advancement of Technology in Finland for a grant.

- [1] W.F. Vinen, *J. Low Temp. Phys.* **145**, 7 (2007) and references there.
- [2] K.W. Schwarz, *Physica B* **197**, 324 (1994).
- [3] R.E. Solntsev *et al.*, *J. Low Temp. Phys.* **147** (2007), arXiv: cond-mat/0607323.

- [4] A.P. Finne *et al.*, J. Low Temp. Phys. **135**, 479 (2004).
- [5] D.C. Samuels, Phys. Rev. B **47**, 1107 (1993).
- [6] A.P. Finne *et al.*, Phys. Rev. Lett. **96**, 85301 (2006).
- [7] A.P. Finne *et al.*, Nature **424**, 1022 (2003).
- [8] A.P. Finne *et al.*, Rep. Prog. Phys. **69**, 3157 (2006).
- [9] R. Hänninen *et al.*, J. Low Temp. Phys. **138**, 589 (2005).
- [10] T.D.C. Bevan *et al.*, J. Low Temp. Phys. **109**, 423 (1997).
- [11] V.B. Eltsov *et al.*, Phys. Rev. Lett. **96**, 215302 (2006).
- [12] The evolution as a function of time is shown in movies at site: <http://ltl.tkk.fi/research/theory/twist.html>
- [13] A.P. Finne *et al.*, J. Low Temp. Phys. **136**, 249 (2004).
- [14] J. Kopu *et al.*, J. Low Temp. Phys. **120**, 213 (2000).
- [15] A.P. Finne *et al.*, J. Low Temp. Phys. **134**, 375 (2004).
- [16] R.J. Zieve *et al.*, J. Low Temp. Phys. **91**, 315 (1993); J. Low Temp. Phys. **90**, 243 (1993).